ACS NANO
Cite This: ACS Nano XXXX, XXX, XXX–XXX
www.acsnano.org

ARTICLE

Oral Nanoparticles Exhibit Specific High-Efficiency Intestinal Uptake and Lymphatic Transport

Kyoung Sub Kim,[†] Kenichi Suzuki,[†,‡] Hana Cho,[†] Yu Seok Youn,[†,§] and You Han Bae*[,†]

[†]Department of Pharmaceutics and Pharmaceutical Chemistry, University of Utah, Salt Lake City, Utah 84112, United States
[‡]Fuji Research Laboratories, Pharmaceutical Division, Kowa Co. Ltd., 332-1 Ohnoshinden, Fuji, Shizuoka 417-8650, Japan
[§]School of Pharmacy, Sungkyunkwan University, Suwon, Gyeonggi-do 16419, Republic of Korea

Supporting Information

ABSTRACT: **Herein, we describe a simple and promising nanoparticle oral delivery phenomenon and propose pathways for oral nanoparticle absorption from the gastrointestinal tract (GIT), combining apical sodium-dependent bile acid transporter-mediated cellular uptake and chylomicron transport pathways. This strategy is proven to employ bile-acid-conjugated, solid fluorescent probe nanoparticles (100 nm diameter) to exclude any potential artifacts and instability issues in observing transport pathways and measuring oral bioavailability. The results of the *in vitro* studies showed that there is no interference from bile acid and no simultaneous uptake of nanoparticles and dextran. The probe nanoparticle exhibited a significantly enhanced average oral bioavailability (47%) with sustained absorption in rats. Particle-size- and dose-dependent oral bioavailability was observed for oral nanoparticle dosing up to 20 mg/kg. The probe nanoparticles appear to be transported to systemic circulation *via* the gut lymphatic system. Thus, we propose a pathway for oral nanoparticle absorption from the GIT, combining apical bile acid transporter-mediated cellular uptake and chylomicron transport pathways.**

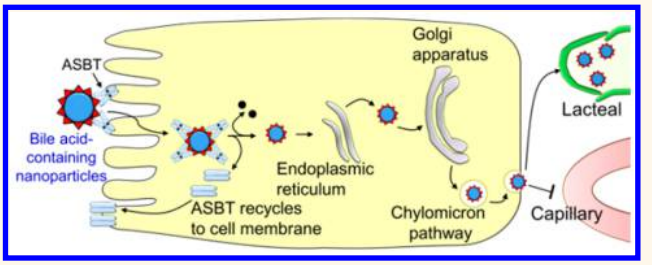

KEYWORDS: *oral drug delivery, nanoparticle intestinal absorption, nanoparticle absorption pathway, nanoparticle lymphatic transport, bile acid transporters*

To date, nanomedicine therapeutic and/or diagnostic products are for parenteral injection, mostly intravenous (IV) administration, although some nasal or pulmonary delivered nanoparticles for alternative, limited applications are known.[1,2] Despite numerous published attempts with various designs, oral insoluble nanoparticles have not proven attractive, primarily due to limited absorption of solid nanoparticles in the intestine.[3] Intact nanoparticles gaining access to the bloodstream *via* gastrointestinal absorption would represent a major breakthrough in the nanomedicine field.[4]

Receptor-mediated endocytosis of solid nanoparticles does occur in the gastrointestinal tract (GIT), depending on particle size, shape, surface, and animal model.[5] Gastric leptin is secreted from epithelial chief cells in gastric mucosa[6,7] and recycled by duodenal enterocytes by clathrin-dependent receptor-mediated endocytosis, followed by transcytotic trafficking through the Golgi network, reaching the GIT basolateral membrane in ~30 min.[8] This process develops vesicles for transcytosis.[6] Cobalamin (vitamin B_{12}; VB_{12}) absorption occurs *via* receptor-mediated endocytosis after binding its gut transporter.[9] Nanoparticles decorated with VB_{12} cause the entry process to switch from clathrin- to caveolae-mediated endocytosis, avoiding lysosomal digestion.[10] However, VB_{12} receptor-mediated nanoparticle delivery suffers from inconsistency and suboptimal plasma concentrations of bioactive agents,[11] due primarily to limited absoprtion capacity of VB_{12}, that is, several micrograms per day for young adults, hardly meeting their desired therapeutic windows.

This long, frustrating history demands an improved paradigm for effective oral delivery technology of nanomedicines. We describe a promising particle oral delivery phenomenon here.

Primary bile acids (BA) and more amphiphilic conjugated BA (cBA) in bile salts are biological surfactants synthesized in the liver from cholesterol and secreted to the duodenum *via* the bile duct and gall bladder to help digest dietary fats.[12] Enterohepatic circulation recycles BA and cBA between the

Received: June 6, 2018
Accepted: July 24, 2018

DOI: 10.1021/acsnano.8b04315
ACS Nano XXXX, XXX, XXX–XXX

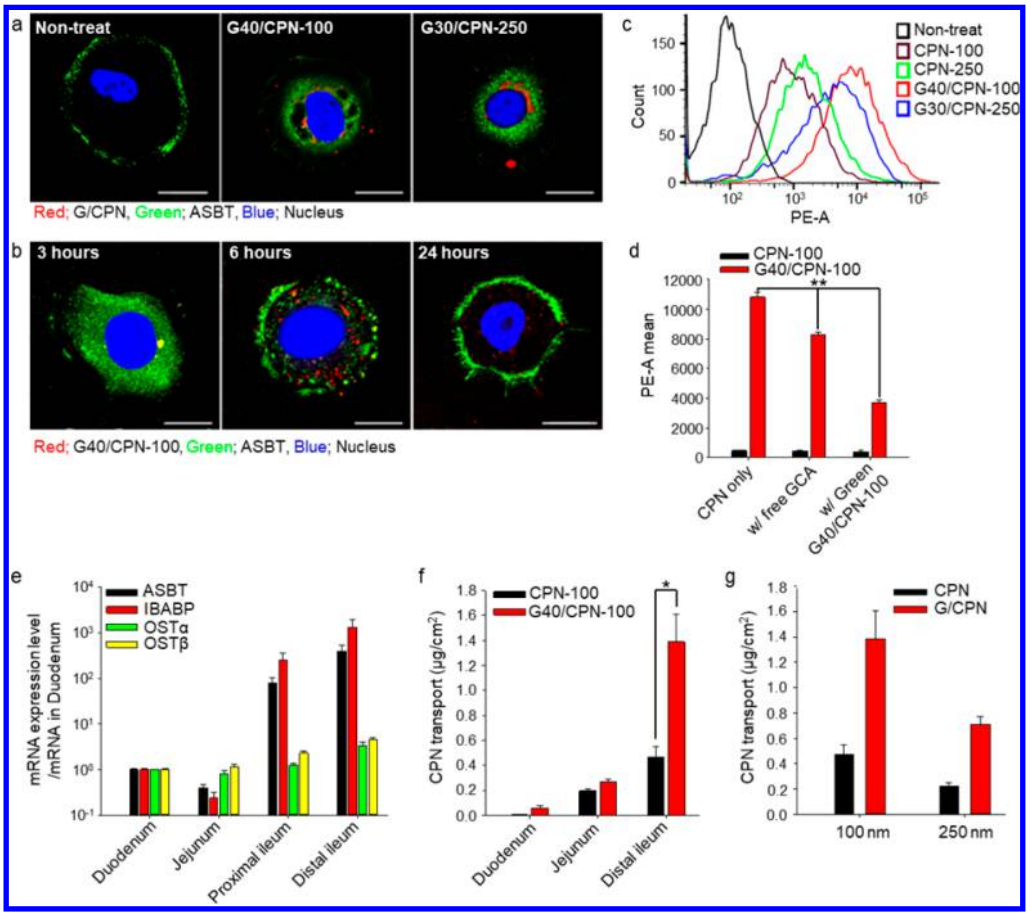

Figure 1. Immunocytochemistry image of G/CPN (red, concentration; 0.1 mg/mL) treated and incubated for (a) 30 min, (b) 3−24 h in SK-BR-3 cells stained with anti-SLC10A2 antibody (green). Cell nucleus stains with DAPI (blue). White scale bar indicates 10 μm. (c) ASBT-mediated cellular uptake efficacy of CPN and G/CPN (concentration; 0.1 mg/mL). (d) Flow cytometry analysis for ASBT-mediated competitive cellular uptake inhibition of G40/CPN-100 (concentration; 0.1 mg/mL) with free GCA (concentration; 1 mg/mL) and green fluorescence (excitation 475 nm; emission 510 nm) G40/CPN-100 (concentration; 0.2 mg/mL) in SK-BR-3 cells (n = 3). (e) BA transporter mRNA expression level in the four different region of small intestine (n = 3). (f) Nanoparticle transport of three different everted gut sac (EGS) tissues (duodenum, jejunum, and distal ileum) in Krebs-Ringer solution containing CPN-100 or G40/CPN-100 (concentration; 50 μg/mL, 37 °C, 90 min incubation) (n = 4). (g) Transport of nanoparticles into on EGS tissue (distal ileum) in Krebs-Ringer solution containing CPN or G/CPN (concentration; 50 μg/mL, 37 °C, 90 min incubation, n = 4); *p < 0.01, **p < 0.001.

GIT and liver with a capacity approximated to be 12−18 g/day in humans.[13,14] Absorptive enterocytes in the distal ileum (ileocyte) and hepatocytes are responsible for BA recycling and are equipped with a series of transporters operating with efficiencies as high as 90−95%.[15] The apical sodium-dependent bile acid transporter (ASBT), the foremost transporter in the ileocyte, is a molecular pump that transforms to a receptor upon contacting soluble macromolecules and drug formulations decorated with BA.[16,17] With the aid of BA, digested fat molecules are absorbed into enterocytes and reassembled back to fat molecules (triglycerides) that are eventually released from enterocytes in a nanoparticle form, together with lipoproteins and cholesterol, and processed by the endoplasmic reticulum (ER) and Golgi apparatus (GA). Resulting fatty nanoparticles (chylomicrons) are moved to systemic circulation *via* the lymphatic system (*i.e.*, cisterna chyli and thoracic duct) and the left subclavian vein.[18]

Here, we provide evidence for substantially improved oral uptake in animals using glycocholic acid (GCA) surface-conjugated solid nanoparticles (G/CPN). The average oral bioavailability (oBA) is 47% for G/CPN with sustained release in orally dosed fasted rats. Similar rat oBAs were observed for oral particle dosing ranging from 1 to 20 mg/kg. Results from *in vitro* and *in vivo* studies support selective particle uptake by ileocyte, minimal interference by free BA, no co-uptake of dextran with G/CPN, and G/CPN size-dependent oBA. G/CPN appears to be transported to systemic circulation *via* the intestinal lymphatic system while avoiding the first pass to the liver.

RESULTS AND DISCUSSION

Commercial carboxylated polystyrene spherical nanoparticles (CPN) of two defined sizes (100 and 250 nm diameters, ζ-potential = −43 and −45 mV) and labeled with red fluorescence were selected as chemically and biologically inert probes which are colloidally stable after GCA conjugation and for minimal nonspecific interactions with anionic biomolecules and cell surfaces in the GIT. Fluorescence intensity was used to trace CPN in biological systems and estimate the nanoparticle concentration in aqueous media, plasma, and lymph using standard curves constructed in each medium. Primary amine groups synthetically introduced to the carboxylate group on GCA were used to couple to carbodiimide-activated carboxyl groups on CPN surfaces

DOI: 10.1021/acsnano.8b04315
ACS Nano XXXX, XXX, XXX−XXX

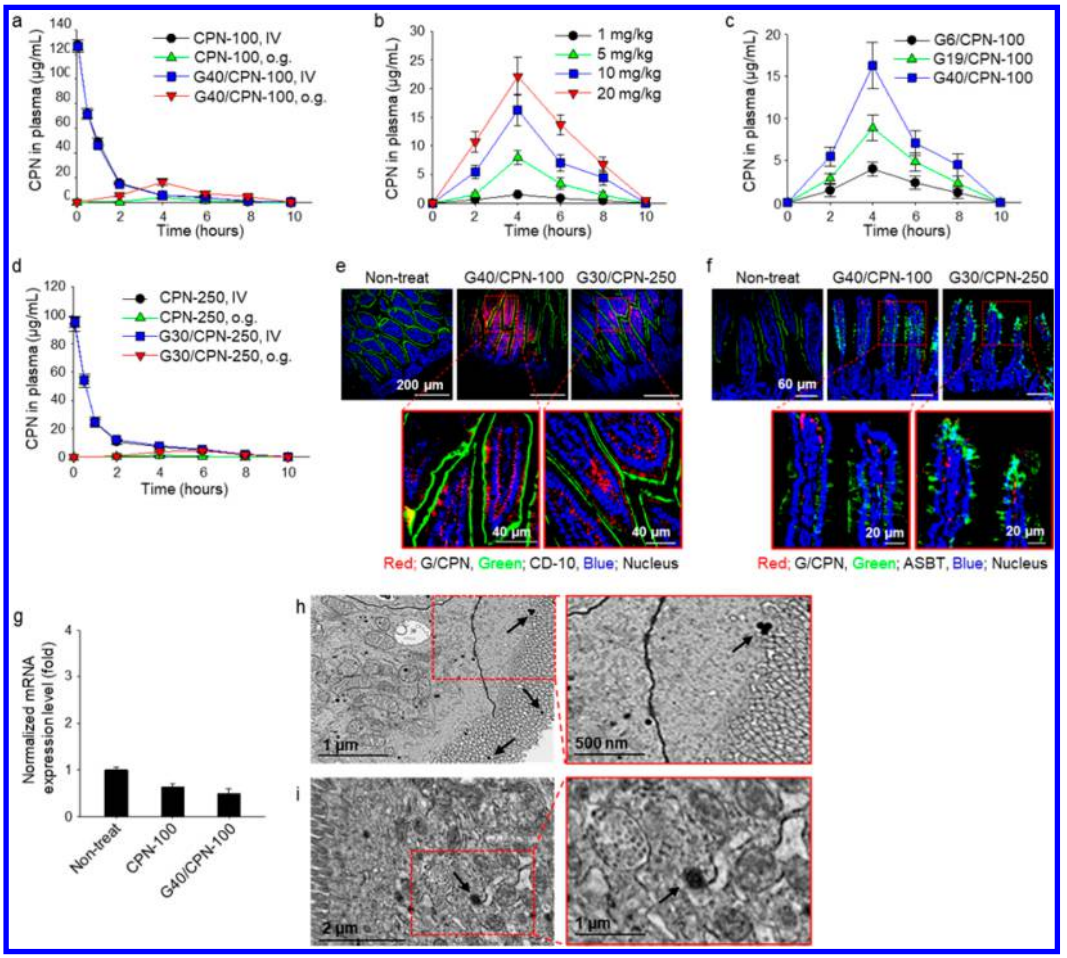

Figure 2. Plasma CPN concentration *versus* time profiles in SD rats: (a) 10 mg/kg of CPN-100 and G40/CPN-100 were administered by IV or o.g. (n = 6). (b) Various doses (1−20 mg/kg) of G40/CPN-100 were administered o.g. (n = 6). (c) Various DS (6−40%) of GCA on CPN-100 were administered o.g. (n = 6). (d) CPN-250 (10 mg/kg) and G30/CPN-250 (10 mg/kg) were administered by IV or o.g. (n = 5). Immunohistochemistry images after distal ileum sacrifice at 4 h postadministration into Balb/c nude mice (10 mg/kg in 0.1 mL water). The harvested distal ileum was stained with (e) anti-CD10 (green) and (f) anti-SLC10A2 antibodies (green). The cell nucleus was stained with DAPI (blue). (g) IBABP mRNA expression level of isolated ileum from 10 mg/kg of CPN-100 and G40/CPN-100 were administered o.g. into Balb/c nude mice (n = 3). These mice were sacrificed after 4 h postadministration. TEM images of distal ileum at 4 h postadministration with (h) 10 mg/kg of G40/CPN-100 and (i) G30/CPN-250 into Balb/c nude mice. Black arrows indicate G/CPN in the distal ileum.

under aqueous conditions (Figure S1a).[19,20] G/CPN formulations were named "G*xx*/CPN-*yyy*", where *xx* and *yyy* are numbers indicating the degree of surface substitution (DS) in % and the size in nanometers of CPN, respectively. The successful modified G40/CPN-100 was confirmed by the ^{1}H NMR spectra, and $-CH_3$ peaks of GCA appeared at 0.5−0.9 ppm (Figure S1b). Characteristics of CPN and G/CPN are summarized in Table S1. The DS was estimated by calculating the surface density of CPN carboxylate groups using titration with Ni^{2+} ion and pyrocatechol violet dye after GCA conjugation.[21] Figure S1c shows transmission electron microscopy (TEM) pictures for CPN-100 and CPN-250 before and after GCA surface modification, showing that they are indistinguishable before and after surface modification. G/CPN from 100 and 250 CPN are stable in water and simulated gastric and intestinal fluids, whereas those from smaller CPN showed limited degrees of aggregation.

A most studied enterocyte BA transporter is the ASBT in the distal ileum. ASBT is expressed by cultured SK-BR-3 cells, staining green when using an antibody against it. ASBT is densely observed on a majority of the cell membrane (Figure 1a). When G/CPN was added to the cell culture medium at a noncytotoxic concentration of 0.1 mg/mL (Figure S1d), cell confocal images reveal that ASBT migrates, concentrating in the perinuclear region along with G/CPN (red dots), but both are not colocalized (Figure 1a). After internalization, ASBT dissociates from G/CPN and slowly recycles to the cell membrane (Figure 1b). Enhanced cellular uptake of G/CPN was observed with GCA surface conjugation (Figure 1c). Cellular G/CPN uptake was inhibited approximately 65% (P value <0.001) under green fluorescence G40/CPN-100 at 2 times higher molar concentration compared to red fluorescence GCA density on G40/CPN-100 surfaces (Figure 1d). G/CPN uptake did not accompany the cellular uptake of soluble macromolecules (cascade blue labeled-dextran, CB-dextran) added to culture media along with G/CPN, despite increasing dextran concentrations up to 0.5 mg/mL (Figure S1e).

Given the lack of accepted monolayer cell culture models representing ileal enterocytes with all transporters, the everted gut sac (EGS) model was used to confirm ASBT-mediated nanoparticle penetration at a tissue level. The expression levels

DOI: 10.1021/acsnano.8b04315
ACS Nano XXXX, XXX, XXX−XXX

Table 1. Pharmacokinetic Analysis of CPN and G/CPN in Rats[a]

formulation	admin route	admin vol (μL)	dose (mg/kg)	T_{max} (h)	C_{max} (μg/mL)	AUC (μg·h/mL$_{(0-10h)}$)	oBA (%)
CPN-100	IV	200	10			146 ± 5	100
CPN-100	o.g.	500	10	4	4.0 ± 0.9	11 ± 3	7 ± 2[d]
G40/CPN-100	IV	200	10			142 ± 5	100
G6/CPN-100	o.g.	500	10	4	4.0 ± 0.8	18 ± 6	13 ± 4[c]
G19/CPN-100	o.g.	500	10	4	8.9 ± 1.5	38 ± 7	27 ± 5[c]
G40/CPN-100	o.g.	500	1	4	1.5 ± 0.4	7 ± 2	47 ± 11[b]
G40/CPN-100	o.g.	500	5	4	8.0 ± 1.3	29 ± 4	40 ± 6[b]
G40/CPN-100	o.g.	500	10	4	16.3 ± 2.8	67 ± 9	47 ± 6[b,d,e]
G40/CPN-100	o.g.	500	20	4	22.1 ± 3.3	107 ± 14	38 ± 5[b]
CPN-250	IV	200	10			112 ± 8	100
CPN-250	o.g.	500	10	4	1.3 ± 0.3	5 ± 1	4 ± 1[e]
G30/CPN-250	IV	200	10			118 ± 7	100
G30/CPN-250	o.g.	500	10	6	4.5 ± 0.8	21 ± 3	18 ± 2[e]
CPN-100 w/cycloheximide	o.g.	500	10	4	3.3 ± 0.9	10 ± 2	7 ± 2[d]
G40/CPN-100 w/cycloheximide	o.g.	500	10	4	5.3 ± 0.8	18 ± 3	13 ± 2[d]

[a]Each value represents the mean ± SEM. C_{max}, maximum plasma concentration; T_{max}, time at which C_{max} is attained; AUC, area under the plasma concentration time curve; oBA, oral bioavailability relative to IV or SC administration. [b]$p > 0.1$. [c]$p < 0.1$. [d]$p < 0.01$. [e]$p < 0.001$.

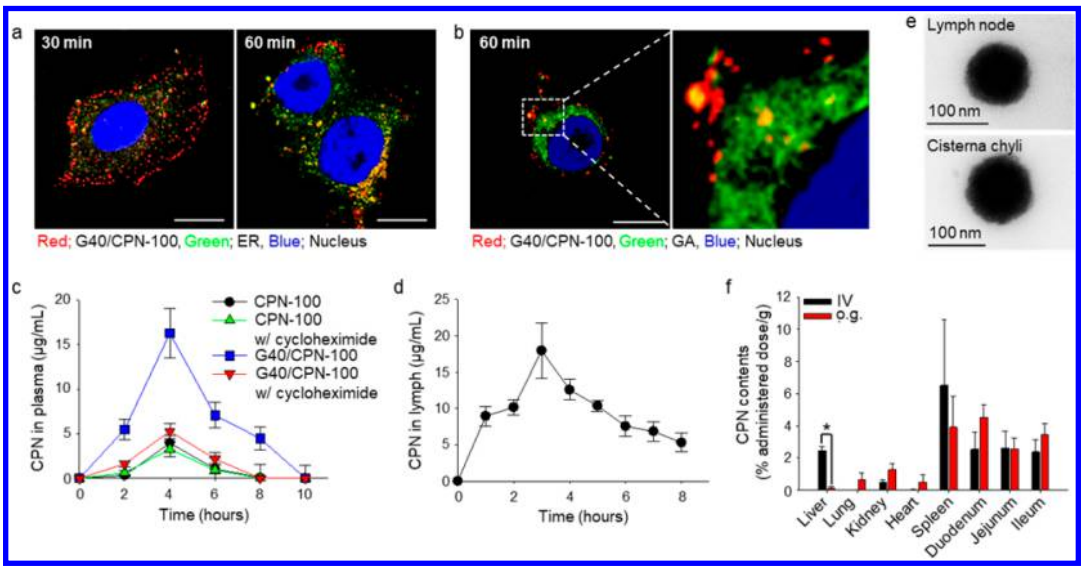

Figure 3. Incubation time-dependent intracellular trafficking images of G40/CPN-100 (concentration; 0.1 mg/mL) treated SK-BR-3 cells. These cells were stained with (a) ER staining kit and (b) GA staining kit. The nucleus is stained with DAPI. White scale bar indicates 10 μm. (c) Plasma CPN concentration *versus* time profiles in SD rats. CPN-100 (10 mg/kg) and G40/CPN-100 (10 mg/kg) were administered o.g. to 3 mg/kg of cycloheximide non- or pretreated (w/cycloheximide) rats (90 min prior to oral CPN administration, $n = 6$). (d) Lymph CPN concentration *versus* time profiles in lymph fistula SD rats. G40/CPN-100 (10 mg/kg) was administered o.g. ($n = 6$). (e) TEM images of abdominal mesenteric lymph node and cisterna chyli at 4 h postadministration with 10 mg/kg of G40/CPN-100 into SD rats. (f) Biodistribution of isolated main organs from 10 mg/kg of G40/CPN-100 was administered by IV or o.g. into SD rat ($n = 5$). These rats were sacrificed after 10 h postadministration of each routes; *$p < 0.001$.

of the BA transporters (ASBT, intestinal bile-acid-binding protein; IBABP, organic solute transporter alpha/beta; OSTα/β) were significantly different in each region of the small intestine, especially in the distal ileum, which showed a significantly larger expression of BA transporters (Figure 1e). Nanoparticle transport in the EGS from the duodenum and jejunum were compared with that from the distal ileum; ileal transport was significantly enhanced (Figure 1f). Control CPN transport at the same time point was 3 times less than G/CPN transport because of nonspecific penetration (Figure 1g). All results support a particle transport mechanism that is primarily specific at the ileocyte, despite a certain fraction of nonspecific transport observed in EGS models. Cellular integrity and tissue viability for 90 min were confirmed by monitoring LDH concentration normalized per unit area of tissue (Figure S1f,g). All LDH concentrations released per unit area were below 40 U/L/cm^2, supporting high tissue viability for the assay time periods.[22]

The pharmacokinetic (PK) study of CPN and G/CPN in Sprague–Dawley (SD) rats was conducted to yield area under the curve (AUC), T_{max}, and C_{max} parameters in plasma. The oBA of oral gavage (o.g.) G40/CPN-100 was calculated with its AUC results relative to its same sample IV administration (Figure 2a). Detailed PK parameters are summarized in Table 1. After the oral dosing of G40/CPN-100 was varied (1, 5, 10, and 20 mg/kg in 0.5 mL sterile water vehicle), the oBA results averaged 47, 40, 47, and 38% (P value >0.1), respectively (Figure 2b). Considering data variation among individual rats

DOI: 10.1021/acsnano.8b04315
ACS Nano XXXX, XXX, XXX–XXX

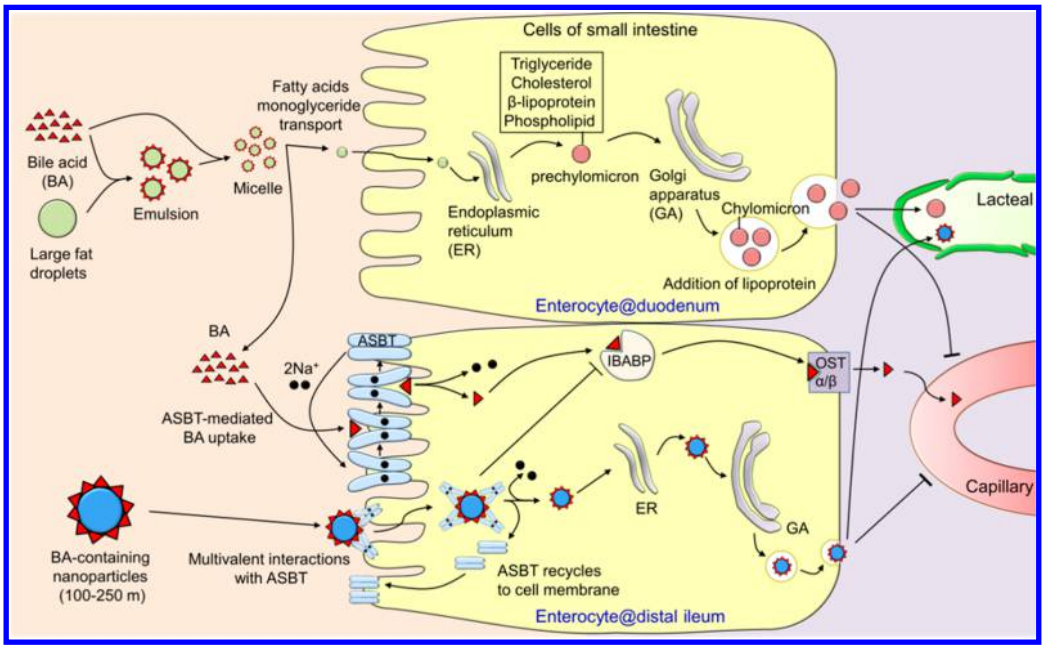

Figure 4. Schematic representation of proposed intracellular trafficking pathway for G/CPN.

and groups, these PK results clearly support consistent oBA and dose-dependent uptake up to 20 mg/kg (Figure S2a–d). These data also show that rat GIT absorption capacity is not rate-limiting over the tested dose range. Changing GCA density on the CPN surface alters oBA: 13% for G6/CPN-100 and 27% for G19/CPN-100 at a dosing of 10 mg/kg (Figure 2c and Figure S2e,f). Particle size also matters: the oBA for a larger nanoparticle, G30/CPN-250, was 18%, which was significantly lower than that of G40/CPN-100 (Figure 2d and Figure S2g), even when considering its lower GCA DS (*i.e.*, 30 *vs* 40%). The reduced oBA observed for G30/CPN-250 can be attributed to limited penetration and/or interactions with dense microvilli (microvillus diameter ∼100 nm). Another interesting finding is that T_{max} for particle plasma concentration for G30/CPN-250 occurs at 5.6 h postadministration, compared to 4 h for G40/CPN-100. Delayed and sustained absorption of nanoparticles may be caused by size-dependent nanoparticle transit times from the esophagus to the ileocyte, interacting with various viscous mucus barriers throughout the entire GIT.[23−25]

Tissues from the distal ileum were isolated from Balb/c nude mice 4 h postadministration with G/CPN oral solutions, fixed, and observed by confocal microscopy to visualize G/CPN in enterocytes after staining tissues green with an antibody against CD-10, a GIT surface enzyme, as seen in Figure 2e. No noticeable tissue differences in CD-10 staining patterns are seen before or after nanoparticle exposure. Upon ASBT antibody tagging, the same tissue apical surface is relatively uniformly stained, similar to CD-10 staining. However, after G/CPN exposure, tissue antibody stain appears to diffuse into the enterocyte, indirectly suggesting ASBT internalization induced by G/CPN (Figure 2f).[26] Notably, G40/CPN-100 did not affect the IBABP expression in the ileum during absorption (Figure 2g, P value >0.1).[27] The presence of G/CPN inside plasma and enterocytes was also confirmed by TEM image (Figure 2h,i and Figure S2h). Ileum tissue morphology after G/CPN oral administration was assessed by hematoxylin and eosin (H&E) staining, and no abnormality in morphology was observed (Figure S2i).

In order to clarify the absorption and transport pathways of G/CPN, the intracellular transport pathway was observed by time and was found to pass through the ER and GA (Figure 3a,b and Figure S3a). The absorption pathway of G40/CPN-100 *via* ER and GA was confirmed through chylomicron flow blockade induced by cycloheximide, which does not affect other absorption pathways.[28] The oBA for G40/CPN-100 significantly decreased to 13% in cycloheximide pretreated rats, indicating the G40/CPN-100 transport to lymphatic vessel through the chylomicron pathway (Figure 3c and Figure S3b). The absorption of G40/CPN-100 to the lymphatic system was clearly confirmed in the lymph fistula rat model (Figure 3d and Figure S3c) and TEM images of the mesenteric lymph node and cisterna chyli (Figure 3e).[29] The absorption pathway through the lymphatic system of G40/CPN-100 can avoid the first pass to the liver (Figure 3f).

Proposed transport pathways based on results shown here for orally dosed G/CPN from GIT to systemic circulation are schematically presented in Figure 4. Digested products of dietary fat (*i.e.*, monoacylglycerols, monoacyl phospholipids, and fatty acids) typically form micelles with BA in the upper GIT.[30] These are largely absorbed as small molecules by active and/or passive uptake mechanisms by duodenal enterocytes,[31] whereas free BA, after delivery of their digested micellar products, is massively recycled at the ileocyte.[13] Orally administered G/CPNs reaching the ileocyte interact with multiple transporters simultaneously on the enterocyte surface (microvilli). Abundant ASBT resident on cell surfaces normally pump free BA into cells by changing conformation upon binding sodium ion and BA.[32] This active process also facilitates direct G/CPN binding *via* GCA. Once attached to the cell surface, more G/CPN binding occurs, enabled by GCA multivalency on G/CPN even in the presence of free BA. Both G/CPN and ASBT are internalized by unknown mechanisms, but co-administered soluble macromolecules are excluded. G/CPN then migrates to cellular perinuclear regions in the ER and GA. After internalization, ASBT dissociates from G/CPN and slowly recycles to the cell membrane. Sodium ion release from ASBT causes ASBT to change its conformation, releasing

DOI: 10.1021/acsnano.8b04315
ACS Nano XXXX, XXX, XXX−XXX

BA.[32] This mechanism may also allow ASBT to release G/CPN. Once located in the enterocyte cytosol, G/CPN seems to share the chylomicron transport pathways in the enterocyte and also follows chylomicron pathways into the systemic blood circulation *via* mesenteric lymph nodes, cisterna chyli, thoracic duct, and the left subclavian vein.

CONCLUSION

In summary, these results support reliable and substantial oral absorption of G/CPN with significant enhanced oBA *via* the GIT BA and chylomicron transport pathways. This is a delivery route for oral nanoparticles, combining two pathways for BA recycling and fat uptake that may not occur naturally. This also provides an approach to the noninvasive and direct delivery of nanomedicine to the central lymphatic system. Accordingly, the route serves as a platform to avoid hepatic toxicity as well as both intestinal and hepatic first-pass metabolisms. Discovery of this GIT penetration route to systemic circulation provides diverse opportunities for direct, noninvasive delivery of nanomedicine to the lymphatic system, allowing immune cell priming before entering the bloodstream. Specific nanoparticle uptake/transport mechanisms by the ileocyte are not fully elucidated and subject to further investigation.

EXPERIMENTAL SECTION

Preparation of Probe Nanoparticles. Prior to conjugation of glycocholic acid (GCA) directly to fluorescent carboxylate polystyrene nanoparticles (CPN, micromod Partikeltechnologie GmbH, Rostock, Germany), the carboxyl group of GCA was modified with ethylenediamine (EDA). GCA (644 μmol) was dissolved in 3 mL of dimethylformamide. Then 838 μmol of *N*,*N*′-dicyclohexylcarbodiimide (DCC), 838 μmol of *N*-hydroxysuccinimide (NHS), and 32.2 mmol of EDA were added to GCA and stirred at room temperature for 24 h. After the reaction, unreacted EDA was removed by rotary evaporation at 80 °C. The reacted solution was precipitated in ethyl acetate and filtered. The collected pellet was dissolved in 10 mL of distilled water and then filtered and lyophilized. Two selected fluorescent (ex = 552/em = 580) 100 nm (CPN-100, 1.9×10^{13} particles) and 250 nm (CPN-250, 1.2×10^{12} particles) CPNs (1% by weight solution) were dispersed in 20 mL of 0.1 M MES buffer at pH 6.0. The CPN was centrifuged for 30 min, at 14 000 rpm, and redispersed in 20 mL of fresh MES buffer twice, and then 1-ethyl-3-(3-(dimethylamino)propyl)carbodiimide hydrochloride (EDC, 30 μmol) and NHS (30 μmol) were added to the CPN solution and stirred for 30 min. The GCA-EDA (0.95−9.5 μmol) was added to the CPN solution and stirred for 24 h. After the reaction, EDC and NHS were purified by centrifugal filter (Mw 10 kDa) at 4000 rpm for 10 min.

Immunocytochemistry. To estimate the optimized concentration of CPN-100 and G40/CPN-100, SK-BR-3 cells (human breast carcinoma, ATCC, HTB 30) were maintained in McCoy's 5a medium containing 10% fetal bovine serum and 1% streptomycin-ampicillin under 5% CO_2 at 37 °C, seeded in 24 wells at a density of 5×10^4 per well. Next, 0.01−1 mg/mL of CPN-100 and G/CPN-100 was treated and incubated for 4 h. After 4 h, cells were washed twice and incubated for 20 h. Then, cell counting kit-8 solution (KB491, Dojindo Laboratories, Kumamoto, Japan) was added to each well, and the plate was continuously incubated for 2 h. The OD value for each well was read at a wavelength of 450 nm to determine the cell viability.

To confirm the G/CPN-mediated ASBT migration and recycle, SK-BR-3 cells were seeded in 6 wells with cover glass at a density of 1×10^5 cell per well. Next, 0.1 mg/mL of G/CPN was treated and incubated for 0.5−24 h. After incubation, cells were washed twice and fixed with 4% paraformaldehyde. Then, cells were stained with anti-SLC10A2 (ab203205, Abcam, Cambridge, MA, USA) and detected with Alexa Fluor 488 conjugated secondary antibodies (ab150077, Abcam, Cambridge, MA, USA). To confirm the intracellular nanoparticle trafficking, 0.1 mg/mL of CPN-100 and G40/CPN-100 was treated and incubated for 5 min. After 5 min, cells were washed twice and continuously incubated for 5−60 min. Then, cells were stained with anti-EEA1 antibody (ab2900, Abacm, Cambridge, MA, USA), Lysotracker green DND-26 (L7526, Invitrogen, Carlsbad, CA, USA), endoplasmic reticulum staining kit (ab139481, Abcam, Cambridge, MA, USA), and Golgi apparatus staining kit (ab139483, Abcam, Cambridge, MA, USA). The nucleus was counterstained with DAPI. The stained cells were analyzed by Olympus FV1000 confocal laser scanning microscopy.

ASBT-Mediated Cellular Uptake. Quantification of CPN and G/CPN absorption efficacy was accomplished by the following procedure. SK-BR-3 cells were seeded in 6 wells at a density of 5×10^5 cells per well. CPN (concentration; 0.1 mg/mL), G/CPN (concentration; 0.1 mg/mL), a mixture of G40/CPN-100 (concentration; 0.1 mg/mL) and free GCA (concentration; 1 mg/mL), a mixture of red fluorescence G40/CPN-100 (concentration; 0.1 mg/mL) and green fluorescence G40/CPN-100 (concentration; 0.2 mg/mL), and a mixture of cascade blue-labeled dextran (CB-dextran, concentration; 0.1−0.5 mg/mL) and G40/CPN-100 (concentration; 0.1 mg/mL) were treated and incubated for 30 min. Then, cells were lifted with DPBS containing 2% FBS (FACS buffer) and washed three times with FACS buffer. A total of 1×10^4 cells per sample were analyzed by flow cytometry (FACS Canto II, BD Biosciences, San Jose, CA, USA), and subsequent data analysis was performed using FlowJo software.

BA Transporters Expression. To measure BA transporters' mRNA expression level in the four different regions (duodenum, jejunum, proximal ileum, and distal ileum) of small intestine, total RNA was extracted from the small intestine using Trizol reagent (Invitrogen) according to manufacturer's instruction and quantified by a spectrophotometer (NanoDrop; Thermofisher scientific). Real-time PCR analysis was performed using cDNA synthesized using RNA (1 μg), dNTP, oligo (dT) 20-mer, and reverse transcriptase (Promega). For real-time PCR reaction, cDNA was mixed with primers and SYBR Green (Thermofisher Scientific), and the samples were analyzed by StepOnePlus real-time PCR system (Applied Biosystem). The gene expression was normalized by mouse β-actin-specific primer-based gene expression level. To measure the CPN- or G/CPN-mediated IBABP mRNA expression in the ileum, 10 mg/kg of CPN and G40/CPN-100 was administrated o.g. to Balb/c nude mice, and then the ileum was harvested 4 h postadministration. Real-time analysis was performed by the above method. The oligonucleotide primer sequences used in these experiments were as follows: mouse IBABP-F 5′-GGC AAG TTC GAG ATG GAG AG-3′ and mouse IBABP-R 5′-TGA GGT CTG GTG ATA GTT GGG-3′; mouse β-actin-F 5′-TAT TGG CAA CGA GCG GTT CC-3′ and mouse β-actin-R 5′-GGC ATA GAG GTC TTT ACG GAT GTC-3′;[27] mouse ASBT-F 5′-TGG GTT TCT TCC TGG CTA GAC T-3′ and mouse ASBT-R 5′-TGT TCT GCA TTC CAG TTT CCA A-3′; mouse OSTα-F 5′-TAC AAG AAC ACC CTT TGC CC-3′ and mouse OSTα-R 5′-GAG GAA TCC AGA GAC CAA A-3′; mouse OSTβ-F 5′-GTA TTT TCG TGC AGA AGA TGC G-3′ and mouse OSTβ-R 5′-TTT CTG TTT GCC AGG ATG CTC-3′.[33]

***Ex Vivo* Nanoparticles Transport Efficacy in the Small Intestine.** All animal experiments were approved by University of Utah's Animal Care and Use Committee. To perform the everted gut sac assay, the small intestine was isolated from 200 to 225 g male Sprague−Dawley rats (Charles River Laboratories International, Inc.). The duodenum, jejunum, and distal ileum were isolated in a length of 5 cm, and each segment was reverted lumen-side out. After one end of the segment was tied, the inner space was filled with oxygenated culture medium (800 μL) and another end was tied to make an EGS with a length of 4 cm. The EGS was placed in a Krebs-Ringer solution (J67591, Alfa Aesar, USA) containing CPN or G/CPN at a concentration of 0.05 mg/mL at 37 °C, and the amount of the CPN transported into each sac was obtained at 90 min.[34] The amount of CPN transported per unit tissue area (calculated by tissue dimension, not surface area expanded by villi and microvilli) was

DOI: 10.1021/acsnano.8b04315
ACS Nano XXXX, XXX, XXX−XXX

analyzed by fluorescence intensity (excitation/emission; 552/580) of CPN with calibration curves in Krebs-Ringer solution.

***In Vivo* Pharmacokinetic Study.** To evaluate the oBA of G40/CPN-100 and G30/CPN-250 in rats, 200−225 g male SD rats were divided into 15 groups (n = 6 for G40/CPN-100, n = 5 for G30/CPN-250). They were fasted for 8 h before and 4 h after administration with free access to water. Blood samples (200 μL) were collected from the jugular vein at 0, 2, 4, 6, 8, and 10 h and then centrifuged (3200 rpm, 4 °C for 10 min) and subsequently quantified by fluorescence intensity with excitation at 552 nm and emission at 580 nm. The calculations of CPN contents in plasma were conducted based on each rat's 0 h fluorescence intensity. Major pharmacokinetic parameters were calculated and compared between test and reference product. The relative oral bioavailability (oBA) value can be expressed by eq 1.[35]

$$\text{oBA} = \frac{\text{AUC(oral)} \times \text{dose(SC or IV)}}{\text{AUC(SC or IV)} \times \text{dose(oral)}} \times 100\% \quad (1)$$

Visualization of Nanoparticles. To clearly visualize CPN oral absorption in ileocytes, 5−6 weeks old Balb/c nude mice (Charles River Laboratories International, Inc.) were maintained under water fasting 8 h before and 4 h after administration. G40/CPN-100 (10 mg/kg) and G30/CPN-250 (10 mg/kg) were administered o.g. After 4 h postadministration, the distal ileum, plasma, the abdominal mesenteric lymph node, and lymph in the cisterna chyli were harvested. The harvested distal ileum was fixed with 2.5% glutaraldehyde and 1% paraformaldehyde in 0.1 M sodium cacodylate buffer overnight. Two different sections were taken from the fixed tissue (i) paraffin sectioned into 5 μm thick slices for immunohistochemistry (IHC), (ii) 70 nm thickness using Leica UC6 Ultratome and collected onto a 200 mesh copper grid for TEM observation. For IHC, the paraffin sections were stained with anti-CD10 (56C6, ab951, Abcam, Cambridge, MA, USA) and anti-SLC10A2 and detected with Alexa Fluor 488 conjugated secondary antibodies (ab150113, ab150077, Abcam, Cambridge, MA, USA). The distal ileum sections were counterstained with DAPI. The stained ileum was analyzed by Olympus FV1000 confocal laser scanning microscopy. The ileum was stained with H&E according to standard protocols.[36] The H&E stained ileum was analyzed using an Olympus BX41 microscope. For TEM imaging, the sections were counterstained by incubation with aqueous saturated uranyl acetate for 10 min followed by staining with lead citrate for 5 min.[37] The harvested lymph nodes were homogenized in PBS. The distal ileum, plasma, homogenized lymph node solution, and lymph from cisterna chyli were observed using TEM (JEOL JEM-1400 Plus operated at 120 kV).

***In Vivo* G/CPN Absorption Pathway.** To evaluate the absorption pathway of G40/CPN-100, 200−225 g male SD rats were pretreated intraperitoneal with cycloheximide (3 mg/kg) dissolved in saline (0.6 mg/mL). After 90 min cycloheximide injection, the G40/CPN-100 (10 mg/kg) was administered o.g. (n = 6). Blood samples (200 μL) were collected from the jugular vein at 0, 2, 4, 6, 8, and 10 h and then centrifuged and subsequently quantified by fluorescence intensity. To confirm nanoparticle lymphatic transport more clearly, the G40/CPN-100 (10 mg/kg) was administered o.g. into a lymph fistula rat model (n = 6).[29] Lymph samples (200 μL) were collected at 0−8 h and then centrifuged (3200 rpm, 4 °C for 10 min) and subsequently quantified by fluorescence intensity. The calculations of CPN contents in lymph were conducted based on each rat's 0 h fluorescence intensity.

Biodistribution Study. To evaluate the biodistribution of G40/CPN-100, 200−225 g male SD rats were fasted for 8 h before and 4 h after administration with free access to water. G40/CPN-100 (10 mg/kg) was administration by intravenous and o.g.. After 10 h postadministration, each major organ (liver, lung, heart, spleen, kidney, duodenum, jejunum, and ileum) was harvested and suspended in PBS and then homogenized to extract CPN. Following centrifugation, the CPN fluorescence intensity in the supernatant was measured (n = 5). The calculations of CPN contents in organs were conducted based on nontreated rat's organ fluorescence intensity.

Statistical Analysis. The results from the *in vitro* studies are expressed as the mean ± standard deviation. The results from the *ex vivo* and *in vivo* studies are expressed as the mean ± standard error of the mean. Differences between the values were assessed using the Student's t test.

ASSOCIATED CONTENT

Supporting Information

The Supporting Information is available free of charge on the ACS Publications website at DOI: 10.1021/acsnano.8b04315.

Preparation and characterization, *in vivo* individual pharmacokinetic absorption, and time-dependent intracellular trafficking images (PDF)

AUTHOR INFORMATION

Corresponding Author

*E-mail: you.bae@utah.edu.

ORCID

You Han Bae: 0000-0002-1488-1924

Notes

The authors declare no competing financial interest.

ACKNOWLEDGMENTS

This work was partially supported by the National Institutes of Health (NIH DK114015-01). The authors appreciate Dr. D.W. Grainger and J. Nichols (University of Utah) for critical comments and suggestions.

REFERENCES

(1) Etheridge, M. L.; Campbell, S. A.; Erdman, A. G.; Haynes, C. L.; Wolf, S. M.; McCullough, J. The Big Picture on Nanomedicine: The State of Investigational and Approved Nanomedicine Products. *Nanomedicine* **2013**, *9*, 1−14.

(2) Anselmo, A. C.; Mitragotri, S. An Overview of Clinical and Commercial Impact of Drug Delivery Systems. *J. Controlled Release* **2014**, *190*, 15−28.

(3) Ensign, L. M.; Cone, R.; Hanes, J. Oral Drug Delivery with Polymeric Nanoparticles: The Gastrointestinal Mucus Barriers. *Adv. Drug Delivery Rev.* **2012**, *64*, 557−570.

(4) Bakhru, S. H.; Furtado, S.; Morello, A. P.; Mathiowitz, E. Oral Delivery of Proteins by Biodegradable Nanoparticles. *Adv. Drug Delivery Rev.* **2013**, *65*, 811−821.

(5) Jung, T.; Kamm, W.; Breitenbach, A.; Kaiserling, E.; Xiao, J.; Kissel, T. Biodegradable Nanoparticles for Oral Delivery of Peptides: Is There A Role for Polymers to Affect Mucosal Uptake? *Eur. J. Pharm. Biopharm.* **2000**, *50*, 147−160.

(6) Bado, A.; Levasseur, S.; Attoub, S.; Kermorgant, S.; Laigneau, J.-P.; Bortoluzzi, M.-N.; Moizo, L.; Lehy, T.; Guerre-Millo, M.; Le Marchand-Brustel, Y.; Lewin, M. J. M. The Stomach Is A Source of Leptin. *Nature* **1998**, *394*, 790−793.

(7) Cinti, S.; De Matteis, R.; Pico, C.; Ceresi, E.; Obrador, A.; Maffeis, C.; Oliver, J.; Palou, A. Secretory Granules of Endocrine and Chief Cells of Human Stomach Mucosa Contain Leptin. *Int. J. Obes.* **2000**, *24*, 789.

(8) Cammisotto, P. G.; Bendayan, M.; Sané, A.; Dominguez, M.; Garofalo, C.; Levy, E. Receptor-Mediated Transcytosis of Leptin Through Human Intestinal Cells in Vitro. *Int. J. Cell Biol.* **2010**, *2010*, 1.

(9) Chalasani, K. B.; Russell-Jones, G. J.; Jain, A. K.; Diwan, P. V.; Jain, S. K. Effective Oral Delivery of Insulin in Animal Models Using Vitamin B12-Coated Dextran Nanoparticles. *J. Controlled Release* **2007**, *122*, 141−150.

DOI: 10.1021/acsnano.8b04315
ACS Nano XXXX, XXX, XXX−XXX

(10) Fowler, R.; Vllasaliu, D.; Trillo, F. F.; Garnett, M.; Alexander, C.; Horsley, H.; Smith, B.; Whitcombe, I.; Eaton, M.; Stolnik, S. Nanoparticle Transport in Epithelial Cells: Pathway Switching Through Bioconjugation. *Small* **2013**, *9*, 3282−3294.
(11) Petrus, A. K.; Fairchild, T. J.; Doyle, R. P. Traveling The Vitamin B12 Pathway: Oral Delivery of Protein and Peptide Drugs. *Angew. Chem., Int. Ed.* **2009**, *48*, 1022−1028.
(12) Russell, D. W. The Enzymes, Regulation, and Genetics of Bile Acid Synthesis. *Annu. Rev. Biochem.* **2003**, *72*, 137−174.
(13) Alrefai, W. A.; Gill, R. K. Bile Acid Transporters: Structure, Function, Regulation and Pathophysiological Implications. *Pharm. Res.* **2007**, *24*, 1803−1823.
(14) Hofmann, A. F. The Continuing Importance of Bile Acids in Liver and Intestinal Disease. *Arch. Intern. Med.* **1999**, *159*, 2647−2658.
(15) Grundy, S. M.; Ahrens, E.; Miettinen, T. A. Quantitative Isolation and Gas−Liquid Chromatographic Analysis of Total Fecal Bile Acids. *J. Lipid Res.* **1965**, *6*, 397−410.
(16) Balakrishnan, A.; Polli, J. E. Apical Sodium Dependent Bile Acid Transporter (ASBT, SLC10A2): A Potential Prodrug Target. *Mol. Pharmaceutics* **2006**, *3*, 223−230.
(17) Dawson, P. A.; Lan, T.; Rao, A. Bile acid transporters. *J. Lipid Res.* **2009**, *50*, 2340−2357.
(18) Tso, P.; Balint, J. Formation and Transport of Chylomicrons by Enterocytes to the Lymphatics. *Am. J. Physiol. Gastrointest. Liver Physiol.* **1986**, *250*, G715−G726.
(19) Byrne, J. A.; Strautnieks, S. S.; Mieli-Vergani, G.; Higgins, C. F.; Linton, K. J.; Thompson, R. J. The Human Bile Salt Export Pump: Characterization of Substrate Specificity and Identification of Inhibitors. *Gastroenterology* **2002**, *123*, 1649−1658.
(20) Craddock, A. L.; Love, M. W.; Daniel, R. W.; Kirby, L. C.; Walters, H. C.; Wong, M. H.; Dawson, P. A. Expression and Transport Properties of the Human Ileal and Renal Sodium-Dependent Bile Acid Transporter. *Am. J. Physiol. Gastrointest. Liver Physiol.* **1998**, *274*, G157−G169.
(21) Hennig, A.; Hoffmann, A.; Borcherding, H.; Thiele, T.; Schedler, U.; Resch-Genger, U. Simple Colorimetric Method for Quantification of Surface Carboxy Groups on Polymer Particles. *Anal. Chem.* **2011**, *83*, 4970−4974.
(22) Surampalli, G.; Nanjwade, B. K.; Patil, P. Safety Evaluation of Naringenin Upon Experimental Exposure on Rat Gastrointestinal Epithelium for Novel Optimal Drug Delivery. *Drug Delivery* **2016**, *23*, 512−524.
(23) Li, D.; Zhuang, J.; He, H.; Jiang, S.; Banerjee, A.; Lu, Y.; Wu, W.; Mitragotri, S.; Gan, L.; Qi, J. Influence of Particle Geometry on Gastrointestinal Transit and Absorption Following Oral Administration. *ACS Appl. Mater. Interfaces* **2017**, *9*, 42492−42502.
(24) Davis, S.; Hardy, J.; Fara, J. Transit of Pharmaceutical Dosage Forms Through the Small Intestine. *Gut* **1986**, *27*, 886−892.
(25) Lai, S. K.; O'Hanlon, D. E.; Harrold, S.; Man, S. T.; Wang, Y.-Y.; Cone, R.; Hanes, J. Rapid Transport of Large Polymeric Nanoparticles in Fresh Undiluted Human Mucus. *Proc. Natl. Acad. Sci. U. S. A.* **2007**, *104*, 1482−1487.
(26) Al-Hilal, T. A.; Chung, S. W.; Alam, F.; Park, J.; Lee, K. E.; Jeon, H.; Kim, K.; Kwon, I. C.; Kim, I.-S.; Kim, S. Y.; Byun, Y. Functional Transformations of Bile Acid Transporters Induced by High-Affinity Macromolecules. *Sci. Rep.* **2015**, *4*, 04163.
(27) Kim, I.; Ahn, S. H.; Inagaki, T.; Choi, M.; Ito, S.; Guo, G. L.; Kliewer, S. A.; Gonzalez, F. J. Differential Regulation of Bile Acid Homeostasis by The Farnesoid X Receptor in Liver and Intestine. *J. Lipid Res.* **2007**, *48*, 2664−72.
(28) Dahan, A.; Hoffman, A. Evaluation of A Chylomicron Flow Blocking Approach to Investigate the Intestinal Lymphatic Transport of Lipophilic Drugs. *Eur. J. Pharm. Sci.* **2005**, *24*, 381−388.
(29) Yoder, S. M.; Kindel, T. L.; Tso, P. Using the Lymph Fistula Rat Model to Study Incretin Secretion. *Vitam. Horm.* **2010**, *84*, 221−249.
(30) Hernell, O.; Staggers, J. E.; Carey, M. C. Physical-Chemical Behavior of Dietary and Biliary Lipids During Intestinal Digestion and Absorption. 2. Phase Analysis and Aggregation States of Luminal Lipids During Duodenal Fat Digestion in Healthy Adult Human Beings. *Biochemistry* **1990**, *29*, 2041−2056.
(31) Westergaard, H.; Dietschy, J. M. The Mechanism Whereby Bile Acid Micelles Increase the Rate of Fatty Acid and Cholesterol Uptake into the Intestinal Mucosal Cell. *J. Clin. Invest.* **1976**, *58*, 97.
(32) Zhou, X.; Levin, E. J.; Pan, Y.; McCoy, J. G.; Sharma, R.; Kloss, B.; Bruni, R.; Quick, M.; Zhou, M. Structural Basis of the Alternating-Access Mechanism in A Bile Acid Transporter. *Nature* **2014**, *505*, 569−573.
(33) Dawson, P. A.; Hubbert, M.; Haywood, J.; Craddock, A. L.; Zerangue, N.; Christian, W. V.; Ballatori, N. The Heteromeric Organic Solute Transporter Alpha-Beta, Ostalpha-Ostbeta, Is an Ileal Basolateral Bile Acid Transporter. *J. Biol. Chem.* **2005**, *280*, 6960−8.
(34) Li, M.; Si, L.; Pan, H.; Rabba, A. K.; Yan, F.; Qiu, J.; Li, G. Excipients Enhance Intestinal Absorption of Ganciclovir by P-gp Inhibition: Assessed *In Vitro* by Everted Gut Sac and *In Situ* by Improved Intestinal Perfusion. *Int. J. Pharm.* **2011**, *403*, 37−45.
(35) Teply, B. A.; Tong, R.; Jeong, S. Y.; Luther, G.; Sherifi, I.; Yim, C. H.; Khademhosseini, A.; Farokhzad, O. C.; Langer, R. S.; Cheng, J. The Use of Charge-Coupled Polymeric Microparticles and Micromagnets for Modulating the Bioavailability of Orally Delivered Macromolecules. *Biomaterials* **2008**, *29*, 1216−1223.
(36) Fischer, A. H.; Jacobson, K. A.; Rose, J.; Zeller, R. Hematoxylin and Eosin Staining of Tissue and Cell Sections. *CSH Protoc.* **2008**, *2008*, pdb.prot4986.
(37) Reynolds, E. S. The Use of Lead Citrate at High pH as an Electron-Opaque Stain in Electron Microscopy. *J. Cell Biol.* **1963**, *17*, 208.

DOI: 10.1021/acsnano.8b04315
ACS Nano XXXX, XXX, XXX−XXX